Eur. Phys. J. Appl. Phys. (2015) 69: 10403
DOI: 10.1051/epjap/2014140335

THE EUROPEAN PHYSICAL JOURNAL
APPLIED PHYSICS

Regular Article

Optimization and tuning of the aspect ratio of hydrothermally grown ZnO nanorods by varying the hydrothermal temperature and their electron transport properties

Kosala Wijeratne[1], Varuni A. Seneviratne[2], and Jayasundera Bandara[1,a]

[1] Institute of Fundamental Studies, Hantana Road, 20000 Kandy, Sri Lanka
[2] Department of Physics, Univeristy of Peradeniya, 20400 Peradeniya, Sri Lanka

Received: 19 August 2014 / Received in final form: 9 October 2014 / Accepted: 22 December 2014
Published online: 27 January 2015 –

Abstract. In this investigation, a facile method to synthesize 1-D ZnO nanorod having different aspect ratio by varying the hydrothermal temperature was demonstrated. The hydrothermal reaction temperatures were optimized to obtain high aspect ratio ZnO nanorods with well-defined 1-D structures. The aspect ratio depended electron transport properties, charge recombination, chemical capacitance, life-time and charge diffusion length of 1-D ZnO nanostructures were investigated. It was observed a clear correlation between the aspect ratio and the electron transport properties of ZnO nanorods. The highest aspect ratio of 7.6 was obtained for the ZnO nanorods synthesized at 100–120 °C and was found to have the highest electron transport properties. It was demonstrated the formation of highly crystalline, high-aspect ratio 1-D ZnO nanorods with enhanced electron transport properties at low hydrothermal temperatures which will be beneficial for device applications.

1 Introduction

In recent past, nanostructured metal oxides such as TiO_2, SnO_2 and ZnO have received great interest mainly due to their favourable physical and chemical properties as well as the availability of cost effective simple fabrication procedures which are environmental friendly [1–3]. The same properties make them much more attractive materials for applications in photonic devices, catalysis, chemical sensors, drug delivery and energy conversion systems [1–3]. Among oxide semiconductor materials, ZnO has been recognized as one of the most important materials which is recognized as a "future material" owing to its ability to grow high quality single crystal and epitaxial layers [4]. ZnO is a direct band gap material having a band gap of 3.2 eV and a large free-exciton binding energy of 60 meV at room temperature [5]. ZnO exhibits multiple properties such as semiconducting, piezoelectric and pyroelectric which makes it wider application in device industry [6].

Several synthesize methods such as chemical deposition [6], hydrothermal [7], spray pyrolysis [8], sol-gel [9], direct current and radio frequency sputtering [10] and pulsed laser deposition [11] have been used to synthesize nanocrystalline films of ZnO nanopowders and 1-D ZnO structures. Among these methods, hydrothermal and sol-gel methods provide many advantages over the other techniques due to simplicity and low equipment cost. Different 1-D ZnO nanostructures such as nanorods [7], nanowires [12], nanotubes [13], tetrapods [14], nanosheets [15], nanobelts [16] and hierarchical structures [17] have been successfully synthesized by the hydrothermal method. These 1-D nanostructures represent the smallest dimension structures that can efficiently transport electrical carriers due to their large surface area to volume ratio. These materials with large surface area to volume ratio are ideal for many nano device applications including ultraviolet photodetectors, sensors, field effect transistors, intramolecular *p*-*n* junction diodes, Schottky diodes, light emitting device, field emitters and gas sensors [18]. As these ZnO 1-D nanostructures play important roles both as interconnect and functional units in fabricating nanoscale electronic and optoelectronic devices, many more wide device applications are found to be emerged. One-dimensional ZnO nanostructures with tuned aspect ratios would be of highly desirable material in device fabrication considering their efficient electron transport properties and enhanced optical characteristics [19]. Different 1-D ZnO nanostructures with varying aspect ratios have been synthesized via hydrothermal method by altering the polarity of the solvents [19], the choice of precursor and precursor concentration [5] changing ionic additives in solution [19] and varying the growth time [20]. By hydrothermal method, ZnO nanowires and nanorods with

[a] e-mail: jayasundera@yahoo.com

sizes and shapes have been successfully synthesized using zinc acetate [17] and zinc nitrate [21] as common precursor materials in different surfactants and complexing agents. Although it has been reported the relationship between the aspect ratio of ZnO nanorods and the hydrothermal temperature, it has not been elucidated in detail [22,23]. In this article, we report the synthesis of ZnO nanorod using zinc acetylacetonate as a single precursor and the dependence of aspect ratio of ZnO nanorods on hydrothermal temperature was investigation in detail. Furthermore, hydrothermal reaction temperature dependent morphology changes and corresponding optical and electrical properties of hydrothermally grown 1-D ZnO nanostructures were explored systematically.

2 Experimental

2.1 Synthesis of ZnO nanorod aggregates and preparation of working electrode

All reagents were analytical grade. 1-D ZnO nanorods were synthesized by a modified method described by Xu et al. [24]. In a typical synthesis, 2.00 g of zinc acetylacetonate hydrate (Aldrich) was dissolved in a 32 mL of ethanol. The solvent was sonicated for complete dissolution of zinc acetylacetonate. Once zinc acetylacetonate was completely dissolved, the solvent was transferred in to a 48 mL of Teflon linear autoclave and heated to a desired temperature (i.e., 100, 120, 140, 160 or 180 °C) for 20 h. Once the reaction is over, the white precipitate was separated by centrifuging after cooling the autoclave. The ZnO nanorod precipitate was subjected to several cycles of washing and re-dispersion with ethanol and finally dried in a vacuum oven. ZnO nanorods synthesized at 100, 120, 140, 160 and 180 °C were labelled as ZnO NR–1, ZnO NR–2, ZnO NR–3, ZnO NR–4 and ZnO NR–5 respectively. The working electrode was fabricated by mixing synthesized ZnO nanorod powder (200 mg) with triton X (10 μL) and ethanol (1 mL) and finally ground well in order to obtain a paste. A thin ZnO nanorod films on FTO glass (Dyesol, sheet resistance 8 Ω/sq) was made by doctor-bladed method and ZnO nanorod coated FTO glass was sintered at 150 °C for 10 min, followed by treating at 300 °C for 15 min and finally sintered at 450 °C for 30 min. These ZnO nanorod films were used as working electrode for all the characterization technique except for band gap measurement. Band gap was measured using powered ZnO nanorods sample by diffuse reflectance method.

2.2 Characterization

The morphologies of the different ZnO nanorods were characterized by scanning electron microscopy (SEM) using a Zeiss Supra 50VP model scanning electron microscopy. UV-vis absorbance spectra were measured by a Shimadzu 2450 UV-vis spectrophotometer. Electrochemical impedance spectroscopy (EIS) measurements (Zahner Zennium electrochemical workstation) were performed under dark condition while the cell was biased at V_{oc}. The AC signal was used with amplitude of 10 mV and frequency of 0.1 Hz–1 MHz range. Mott-Schottky analysis was performed in a three-electrode cell. The ZnO photoanode was used as the working electrode, a Ag/AgCl electrode served as the reference electrode, and platinum wire was used as the counter electrode. Mott-Schottky measurements were acquired with a Zahner Zennium electrochemical workstation. In all cases, a 10 mV sinusoidal excitation signal was employed to interrogate the capacitance. Capacitance was determined from two-frequency measurements at low and high frequencies. The structural properties of ZnO NR films were determined by using Seimens D5000, X-ray diffractometer with advance rotaflex diffraction meter using Cu Kα radiation and $\lambda = 1.5406$ Å. Crystallite size was calculated using Debye-Scherrer formula [25], $d = 0.89\lambda/\beta\cos(\theta)$, where, 0.89 is Scherrer's constant, λ is the wavelength of X-rays, θ is the Bragg diffraction angle and β is the full width at half-maximum (FWHM) of the diffraction peak corresponding to plane $\langle 1\,0\,1\rangle$ of ZnO nanorods.

3 Results and discussion

In this work, we synthesized ZnO nanorod by hydrothermal technique varying the hydrothermal reaction temperature. The main focus of the investigate was to study the effect of hydrothermal temperature on the aspect ratio of ZnO nanorods and to ascertain the aspect ratio dependence electronic as well as physical properties of 1-D ZnO nanorods. In hydrothermal conditions, following simplified chemical reactions may have been involved in the formation of ZnO nanorods [19].

$$Zn^{2+} + 2OH^- \rightarrow Zn(OH)_2 \tag{1}$$

$$Zn(OH)_2|2OH^- \rightarrow [Zn(OH)_4]^{2-} \tag{2}$$

$$Zn(OH)_2 \leftrightarrow ZnO + H_2O \tag{3}$$

$$[Zn(OH)_4]^{2-} \leftrightarrow ZnO + H_2O \tag{4}$$

As the initiation step, hydrolysis of zinc acetylacetonate by OH^- ions which are obtained by the deprotonation reaction of H_2O molecules produces $Zn(OH)_2$ and $[Zn(OH)_4]^{2-}$. According to Kuriakose et al., in a neutral or weakly basic solution, Zn^{2+} forms $Zn(OH)_2$ and $[Zn(OH)_4]^{2-}$ by reactions (1) and (2) [26]. The growth unit $[Zn(OH)_4]^{2-}$ plays a key role in the ZnO nanorods formation under hydrothermal conditions where several dissolution-nucleation cycles given by equation (4) results in formation of ZnO nanorods. As ZnO is a polar crystal, the growth along the $[0\,0\,0\,1]$ direction was enhanced in a polar solvent such as ethanol, resulting in formation of rod-like ZnO morphologies. In addition, it has been reported that the precursor acetylacetonate has a templating role giving the hexagonal arrangement of primary

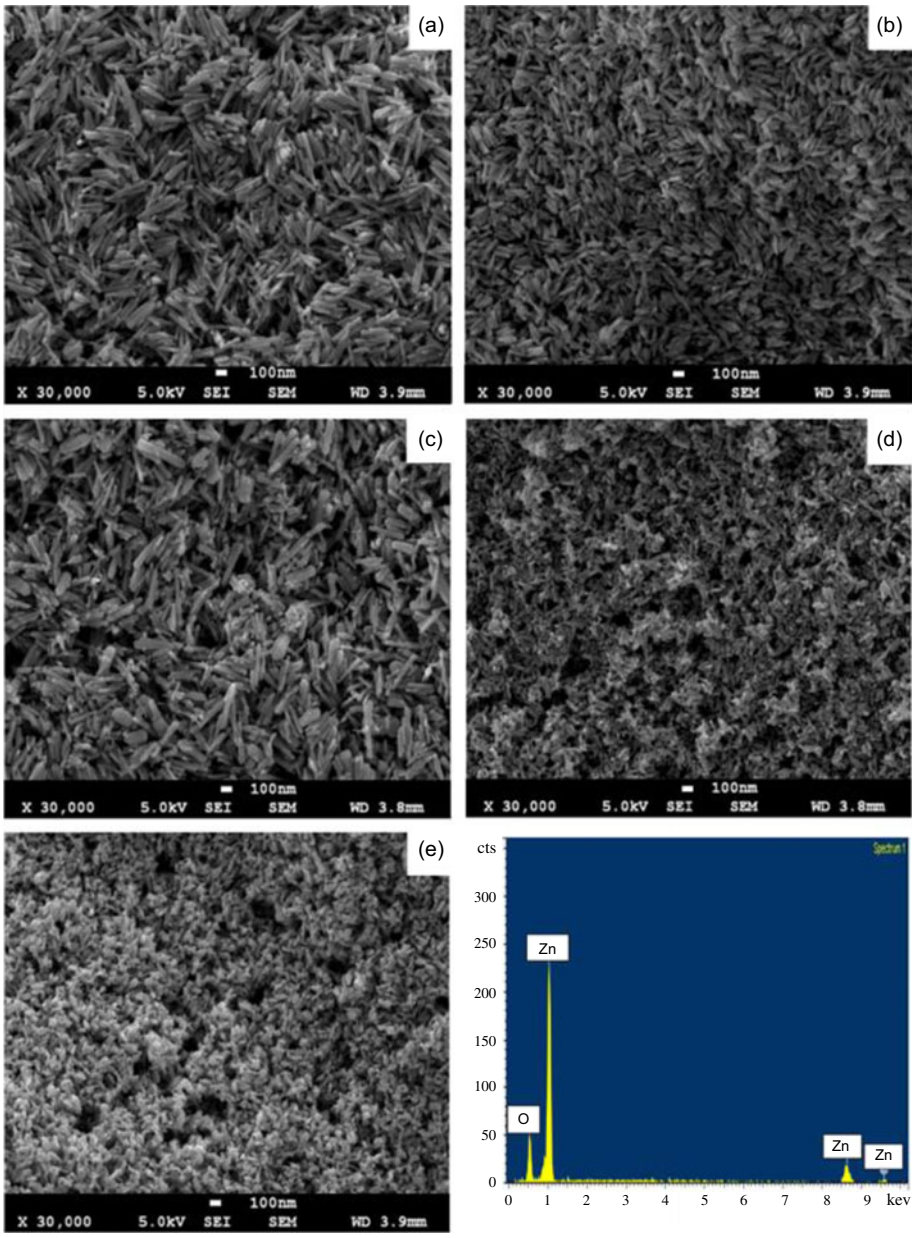

Fig. 1. Surface SEM images of (a) ZnO NR–1, (b) ZnO NR–2, (c) ZnO NR–3, (d) ZnO NR–4, (e) ZnO NR–5, (f) EDX spectrum of ZnO NR films.

ZnO particles which aggregates in stable hexagons and then grow hierarchically with time [27]. These observations indicate that the growth process of ZnO nanorods can be controlled by varying the ZnO preparation conditions such as precursor concentration, growth temperature and growth time. By judicial choice of precursor concentration, the density of ZnO nanorods can be optimized while the aspect ratio and morphology of ZnO nanorods can be adjusted by optimizing the growth time and temperature.

In this report, the effect of hydrothermal temperature on the aspect ratio of ZnO nanorods was investigated. SEM analysis of the ZnO nanorods synthesized at different hydrothermal temperatures revealed that the formation of 1-D ZnO nanorods was initiated only at 100 °C. Figures 1a–1e show the SEM images of ZnO nanorods synthesized at 100, 120, 140, 160 and 180 °C respectively. As shown in Figure 1, formation of cylindrical type of ZnO nanorods is evident in all the temperatures. Additionally, aggregation of random ZnO nanorods are observed at higher hydrothermal temperatures (160 °C and 180 °C) where as in other cases, formation of clusters/bundles of nanorods was noticed. SEM images shown in Figure 1 clearly demonstrate the dependence of the length and the diameter of ZnO on the hydrothermal temperature where at low and high hydrothermal temperatures, longer and shorter ZnO nanorods were formed respectively. That is at 100 °C, the length and diameter of ZnO nanorods are ∼330 nm and ∼43 nm respectively while at 180 °C, the length and the diameter of ZnO nanorods are ∼103 nm

Table 1. Calculated nanorod lengths, diameter and aspect ratios of ZnO NRs with the hydrothermal temperature.

Sample	Avg. length with stan. deviation/nm	Avg. diameter with stan. deviation/nm	Aspect ratio
ZnO NR–1	329.6 ± 20	43.1 ± 5	7.6
ZnO NR–2	283.2 ± 23	41.3 ± 5	6.8
ZnO NR–3	179.2 ± 21	30.4 ± 4	5.9
ZnO NR–4	126.8 ± 21	23.4 ± 5	5.4
ZnO NR–5	103.0 ± 14	23.3 ± 6	4.4

and ∼23 nm respectively. The length and the diameter of the ZnO nanorod were estimated by averaging 50 nanorods in a selected area of the SEM image. The estimated nanorod lengths, diameters and aspect ratios of different 1-D ZnO nanostructures formed at 100, 120, 140, 160 and 180 °C are given in Table 1. As given in Table 1, the aspect ratio of ZnO nanorod is found to decrease with the increase of hydrothermal temperature where the highest aspect ratio of 7.6 and the lowest aspect ratio of 4.4 were observed for the ZnO nanorods synthesized at 100 and 180 °C respectively.

As shown by SEM images, the aspect ratio of ZnO nanorods decreases as the hydrothermal temperature increases from 100 to 180 °C and the dependence of aspect ratio of 1-D ZnO nanorods on hydrothermal temperature can be explained as follows; when a polar solvent such as ethanol was used as the solvent, the increase in hydrothermal temperature results in rapid increase in the saturated vapour pressure in the reaction vessel. Under high-pressure conditions, the growth of the ZnO nuclei may perhaps be restricted due to dissolution of ZnO nuclei (reaction 5) which could result in formation of ZnO nanorods with shorter lengths and diameters at higher hydrothermal temperatures than that of lower hydrothermal temperatures.

$$[\mathrm{Zn(OH)_4}]^{2-} = \mathrm{Zn}^{2+} + 4\mathrm{OH}^{-}\ (\text{dissolution}) \qquad (5)$$

Additionally, we have noticed the formation of clusters or aggregation of ZnO nanorods and even secondary structures such as ZnO nanoparticles at higher hydrothermal temperatures (Figs. 1d–1e).

High aspect ratio ZnO nanorods are important materials in device applications due to their enhanced electronic as well as optical properties. Hydrothermal temperature depended electronic as well as physical properties of ZnO nanorods were elucidated in the following sections. The crystalline structures of products were determined by XRD analysis and the X-ray diffraction patterns of ZnO nanorods synthesized at 100, 120, 140, 160 or 180 °C are shown in Figure 2. The diffraction peaks seen at 31.84°, 34.52°, 36.33° and 47.63° could be indexed as hexagonal wurtzite phase of ZnO with lattice constants $a = b = 0.324$ nm and $c = 0.521$ nm (JPCDS card number: 36-1451) [19]. The additional peak seen at 37.8° of the diffraction patterns of ZnO nanorods could be due to an impurity. Interestingly, the crystalline structure of the ZnO nanorods prepared at different hydrothermal

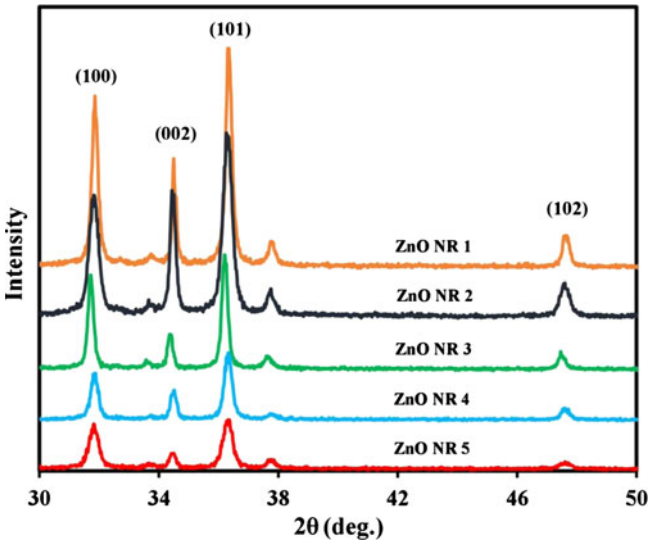

Fig. 2. XRD patterns of ZnO NR films of (A) ZnO NR–1, (B) ZnO NR–2, (C) ZnO NR–3, (D) ZnO NR–4 and (E) ZnO NR–5.

temperatures appeared to be the same. Additionally, the crystallite size calculated using Debye-Scherrer formula [25], indicates a crystallite size of ∼22.3 nm for the ZnO nanorods synthesized at 100–120 °C while a crystallite size of ∼22.9 nm for the ZnO nanorods synthesized at 140–160 °C. These results show that the hydrothermal temperature plays a minor role on controlling the crystallite size though it has a significant effect on control of lengths and diameters of ZnO nanorods.

Band gap energies and the light scattering ability of the ZnO nanorods synthesized at different hydrothermal temperatures were measured by UV-vis diffuse reflectance spectra. The band gaps of the ZnO nanorod based films were determined by optical absorption near the band edge from $\alpha h\nu$ vs. $A(h\nu - E_g)^{n/2}$ plot by extrapolation the straight line to the x-axis where α, $h\nu$, A and E_g are optical absorption coefficient, the photonic energy, proportionality constant, and band gap respectively. As shown in the Figure 3a, it is evident the decrease of the band gap of ZnO nanorods from 3.20 to 3.15 eV as the hydrothermal temperature increases from 100 °C to 180 °C. However, as described earlier, X-ray diffraction analysis indicated the same crystallite size for ZnO nanorods synthesised at 100–180 °C. This type of slight discrepancy may be attributed to the electron-electron, electron impurity scattering [28] and different light scattering properties of different ZnO nanorods. The variation of light scattering properties of ZnO nanorods with the change of hydrothermal temperature is shown in Figure 3b. For light scattering measurements described in Figure 3b, identical thick films consisting of ZnO nanorod synthesized at 100, 120, 140, 160 or 180 °C were employed. As shown in Figure 3b, ZnO nanorods synthesized at higher hydrothermal temperatures exhibit higher light scattering properties than that of ZnO synthesized at lower hydrothermal temperatures. Especially a very notable higher light scattering enhancement is observed in the 400–800 nm

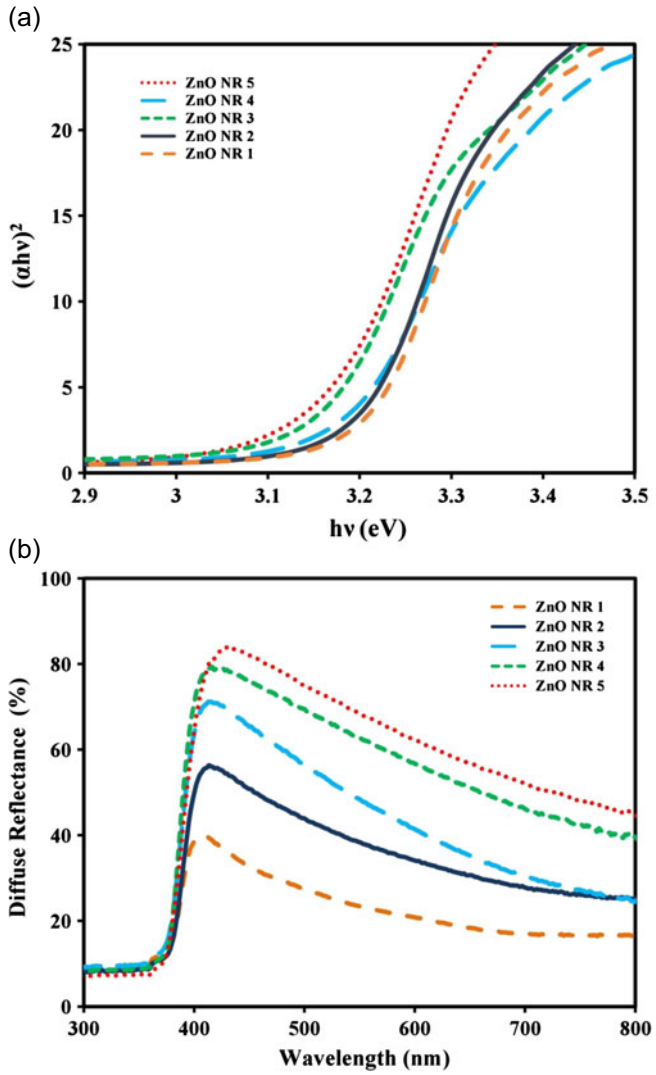

Fig. 3. (a) Tauc plot and (b) diffuse reflectance of ZnO NR films of ZnO NR films of (A) ZnO NR–1, (B) ZnO NR–2, (C) ZnO NR–3, (D) ZnO NR–4 and (E) ZnO NR–5 prepared by doctor-blade method.

region in the case of ZnO synthesized at higher hydrothermal temperatures. Mainly, significant optical absorption properties of nanorods of different diameters were clearly noticeable in Figure 3b. The absorption intensity increased with decreasing ZnO nanorod diameter, and the highest absorption intensity was observed for ZnO nanorods synthesised at 180 °C and the high absorption intensity was attributed to high light scattering effect smaller diameter ZnO nanorods [29]. On the other hand, the observed enhanced light scattering of ZnO nanorods synthesised at higher temperatures could be due to closely packing of shorter ZnO nanorods formed at higher hydrothermal temperatures. Such an enhanced light scattering ability is a very useful property especially in photovoltaic devices fabrication.

The energy positions and donor densities (N_d) of semiconductors are important parameters when semiconductors are used for device fabrication which could be extracted from the capacitance measurements. Mott-Schottky plots

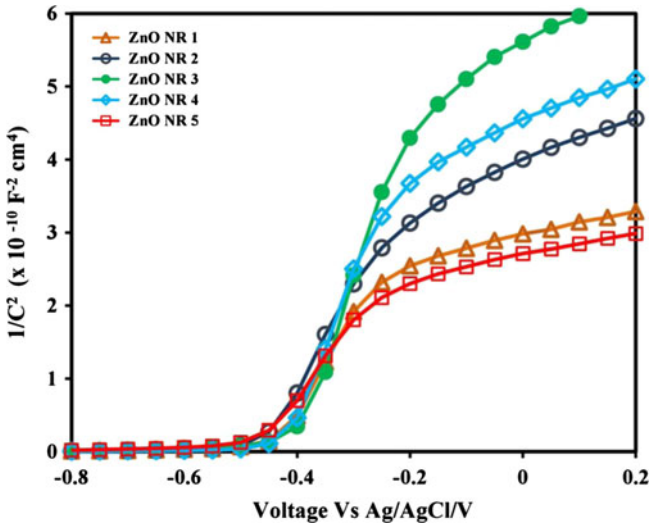

Fig. 4. Mott-Schottky plots of ZnO NR films ZnO NR films (A) ZnO NR–1, (B) ZnO NR–2, (C) ZnO NR–3, (D) ZnO NR–4 and (E) ZnO NR–5.

of different ZnO nanorods synthesized at 100, 120, 140, 160 or 180 °C are shown in Figure 4. According to the capacitance data shown in Figure 4, the flat-band potential (V_{fb}) could be obtained from the x-intercept of the linear region of the curve C^{-2} vs. V while N_d could be obtained from the equation (6). In equation (6), e is the electronic charge unit, ε_0 is the permittivity of free space, ε is the dielectric constant, N_d is the dopant density (cm^{-3}), V is the applied potential (V) and C is the capacitance [30].

$$N_d = -\left(\frac{2}{e\varepsilon_0\varepsilon}\right)\left(\frac{d\left(1|C^2\right)}{dV}\right). \quad (6)$$

The measured V_{fb} and N_d of ZnO nanorods synthesized at different hydrothermal temperatures are given in Table 2. The dopant density results given in Table 2 revealed a dramatic decrease in N_d of ZnO nanorods as the hydrothermal temperature increases from 100 to 180 °C. Similarly, as shown in Figure 4, a slight negative shift in V_{fb} of ZnO nanorods is noted with the decrease of hydrothermal temperature. As it is known, the negative shift in V_{fb} of metal oxides nanoparticles is owing to accumulation of charges [31], the observed negative shift in V_{fb} of ZnO nanorods synthesized at low temperature could be assigned to enhanced N_d due to formation of oxygen vacancies in ZnO nanorods synthesized at lower hydrothermal temperatures. The Mott-Schottky results presented above for ZnO nanorods synthesized at different hydrothermal temperature revealed a larger N_d and more negative V_{fb} potentials for those ZnO nanorods synthesized at lower hydrothermal temperatures. A larger N_d and more negative V_{fb} are very important properties especially for solar cell fabrication as they control the charge transport and open circuit voltage respectively.

It is well-known that the electron transport, charge recombination as well as diffusion coefficient of ZnO

Table 2. Carrier density and flat band potential of ZnO NR films with the variation of hydrothermal temperature.

Hydrothermal temperature (°C)	N_d (cm^{-3})	V_{fb} (V)
100	1.54×10^{20}	−0.46
120	1.30×10^{20}	−0.45
140	1.23×10^{20}	−0.43
160	0.97×10^{20}	−0.42
180	0.78×10^{20}	−0.39

nanostructures depend on the synthesis method [31]. Electron transport and recombination properties of ZnO nanorods synthesized with the variation of hydrothermal temperature were investigated by EIS method which is a well-known technique to investigate the interfacial charge transfer properties [32,33]. Figure 5 shows the Nyquist plots of ZnO nanorods electrodes fabricated with different hydrothermal temperatures obtained at −0.30 V vs. Ag/AgCl in 0.5 M $NaClO_4$ solution in the dark where impedance measurements were performed by applying a 10 mV AC signal over the frequency range of 0.1 Hz–1 MHz. In the Nyquist plot shown in Figure 5, the large semicircle in the low-frequency regions is associated with the charge transfer at the ZnO/electrolyte interface (R_k). In addition, the charge transport resistance (R_w) which is overlapped with the R_k, represents how effectively charge transport through the ZnO nanorod network. EIS results presented in Figure 5 were fitted in terms of equivalent circuits corresponding to the transmission line model shown in the inset in Figure 5. From these fitted results, chemical capacitance (C_μ), charge-transfer (recombination) resistance (R_k) and the electron transport resistance R_w can be calculated and these parameters are directly related to the electron diffusion coefficient (D_n), and diffusion length (L_n) of ZnO nanorod electrodes [31].

The estimated C_μ, R_k, R_w, D_n and L_n of ZnO nanorod synthesized at 100, 120, 140, 160 or 180 °C are given in Table 3. As given in Table 3, R_k increases with the increase of hydrothermal temperature suggesting less charge recombination at the ZnO/electrolyte interface for the ZnO nanorods synthesized at higher hydrothermal temperatures than lower hydrothermal temperatures. At the same time, R_w of ZnO nanorods found to be increased with the increase of hydrothermal temperature resulting in slightly reduced electron transport properties for the ZnO nanorods prepared at higher hydrothermal temperatures. The observed behaviour of R_k and R_w of ZnO nanorods can be correlated to the N_d as the electron transport properties and charge recombination properties of oxide semiconductors are associated with the charge

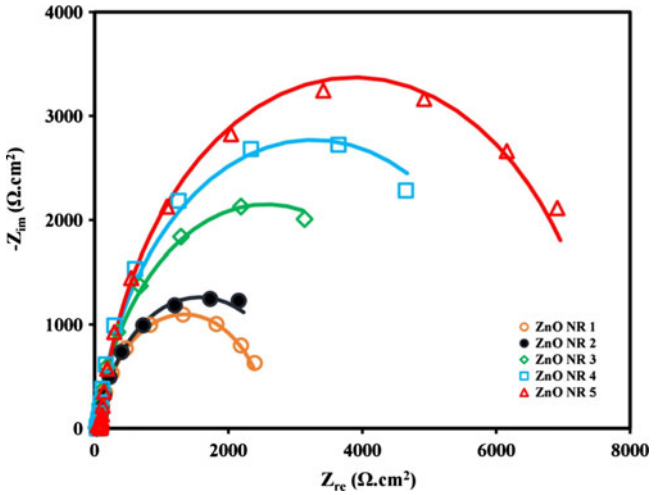

Fig. 5. Nyquist plot of ZnO NR films (A) ZnO NR–1, (B) ZnO NR–2, (C) ZnO NR–3, (D) ZnO NR–4 and (E) ZnO NR–5 obtained at −0.30 V vs. Ag/AgCl in the 0.5 M $NaClO_4$ solution in the dark.

carrier density of the nanostructures [34]. By Mott-Schottky analysis, it was demonstrated the greater N_d for ZnO nanorods synthesized at lower hydrothermal temperatures than that of ZnO nanorods synthesized at higher hydrothermal temperatures. The observed larger N_d for the ZnO nanorods synthesized at lower hydrothermal temperatures could be due to creation of a large number of oxygen vacancies and surface states in ZnO nanorods during synthesis of ZnO nanorods at lower hydrothermal temperatures. These oxygen vacancies are known to act as electron donors creating large dopant density. These surface states or oxygen vacancies in semiconductor nanoparticles have ability to enhance the electrical conductivity as well as the electron transfer at the semiconductor interface. Hence, observed enhanced charge recombination resistance (R_k) and charge transport resistance (R_w) of ZnO nanorods synthesized at higher hydrothermal temperatures can be justified.

Furthermore, it was shown the formation of aggregates of ZnO nanorods at higher hydrothermal temperatures and these aggregation will be unfavourable for free movement of electrons in the ZnO nanorod network and hence observed higher R_w for ZnO nanorods at higher hydrothermal temperatures can be justified. Additionally, enhanced electron transport properties could expect for high aspect ratio ZnO nanorods due to their one-dimensional nature which provide direct and short pathways for charge transport compared to low aspect

Table 3. Variation of charge transport parameters of ZnO NR films (film thickness ≈12 μm) with the hydrothermal temperature.

Temperature (°C)	R_k(Ω cm^2)	R_w(Ω cm^2)	C_μ (μF cm^{-2})	D_n (cm^2 s^{-1}) × 10^{-4}
100	2070	0.84	110.15	15.6
120	3030	1.19	104.50	11.6
140	5050	1.81	94.34	8.39
160	6430	3.03	59.78	7.95
180	7570	6.55	29.03	7.57

ratio ZnO nanorods synthesized at higher hydrothermal temperature.

The other important parameter of semiconductor materials is the chemical capacitance (C_μ). A higher chemical capacitance was observed for the ZnO nanorods synthesized at lower hydrothermal temperatures than higher hydrothermal temperatures. The capacitance measurements provide important information on the density of states (DOS) and the electron density of the materials. The C_μ can be expressed by the following equation:

$$C_\mu = \frac{q^2 \alpha n L}{k_b T} \exp\left(\frac{\alpha\,(E_F - E_C)}{k_b T}\right), \tag{7}$$

where k is the Boltzmann constant, T is the temperature and q is the electron charge. As given in Table 3, the C_μ of the ZnO nanorods prepared at lower hydrothermal temperatures is higher than that of ZnO nanorods prepared at higher hydrothermal temperatures. A higher C_μ indicates the higher electron concentration in ZnO nanorods prepared at lower hydrothermal temperatures and hence higher electron transport properties of ZnO nanorods prepared at lower hydrothermal temperatures can be further justified [32,33,35].

Moreover, higher electron diffusion coefficients/lengths and superior life-times were observed for ZnO nanorods synthesized at lower hydrothermal temperatures. The electron diffusion coefficient (D_n) was calculated by the following equation (8), where L is film thickness of the ZnO nanorod film. The calculated D_n results given in Table 3 indicate that the ZnO nanorods synthesised at lower hydrothermal temperature have higher D_n than that of ZnO synthesized at higher hydrothermal temperatures which will favour transport of electrons for long distance with less hindrance. Likewise, the electron diffusion length (L_n) represents the distance that electrons travel on average before they recombine with electron acceptors and L_n is represented by the equation (9). The calculated L_n values for ZnO nanorods synthesized at 100, 120, 140, 160 or 180 °C are given in Table 3. The significant higher L_n values observed for the ZnO nanorods synthesized at 100–140 °C can be attributed to the properties like aspect ratio of ZnO nanorods as electron diffusion and hence electron diffusion lengths can be augmented by the presence of high aspect ratio ZnO nanorod structures. This observation implies that the charge transport would be better for ZnO nanorods synthesized at low temperatures than that of the ZnO nanorods synthesized at higher temperatures.

$$D_n = \frac{L^2}{R_w C_\mu}, \tag{8}$$

$$L_n = L\sqrt{\frac{R_k}{R_w}}. \tag{9}$$

4 Conclusion

We have shown that the aspect ratio of ZnO nanorod can be optimised by varying the hydrothermal temperature. High and low aspect ratio ZnO nanorods were synthesized at temperature ranges of 100–120 °C and 160–180 °C respectively. Formation of ZnO nanorods was not observed when the hydrothermal temperature was below 100 °C. Characterizations of these ZnO nanorods indicate that the high aspect ratio one-dimensional ZnO nanorods with single-crystalline structure having high chemical potential and high dopant density can provide a direct path for charge carrier transport, resulting in small electron transport resistance (R_w) and long electron diffusion length (L_n). On the other hand, low aspect ratio ZnO nanostructrues, with low chemical potential and lower dopant density found to be having higher interfacial charge recombination resistance.

References

1. S. Xu, Z.L. Wang, Nano Res. **4**, 1013 (2011)
2. J. Yu, Y. Wang, W. Xiao, J. Mater. Chem. A **1**, 10727 (2013)
3. M. Yang et al., Nano Res. **4**, 901 (2011)
4. M. Distaso et al., Nanoscale **4**, 864 (2012)
5. C.-M. Wu et al., J. Phys. Chem. C **115**, 10164 (2011)
6. B. Cao, W. Cai, J. Phys. Chem. C **112**, 680 (2008)
7. B. Liu, H.C. Zeng, J. Am. Chem. Soc. **125**, 4430 (2003)
8. A. Douayar et al., Eur. Phys. J. Appl. Phys. **53**, 20501 (2011)
9. S. Kumar et al., J. Phys. Chem. C **116**, 16700 (2012)
10. T. Minami, H. Nanto, S. Takata, Thin Solid Films **124**, 43 (1985)
11. C.V. Manzano et al., J. Phys. Chem. C **117**, 1502 (2013)
12. P. Jiang et al., Adv. Funct. Mater. **17**, 1303 (2007)
13. Y. Sun, D.J. Riley, M.N. Ashfold, J. Phys. Chem. B **110**, 15186 (2006)
14. O. Lyapina et al., Inorg. Mater. **44**, 846 (2008)
15. S. Zhu et al., RSC Advances **3**, 2910 (2013)
16. L. Nasi et al., Nanoscale **5**, 1060 (2013)
17. X. Wang et al., J. Phys. Chem. C **115**, 2769 (2011)
18. Z.L. Wang, J. Phys.: Condens. Matter **16**, R829 (2004)
19. B. Cheng et al., Inorg. Chem. **45**, 1208 (2006)
20. G. Amin et al., J. Nanomater. **2011**, 5 (2011)
21. X. Zhou et al., Physica E **43**, 1056 (2011)
22. S. Xu et al., ACS Nano. **3**, 1803 (2009)
23. D. Polsongkram et al., Physica B: Condens. Matter **403**, 3713 (2008)
24. L. Xu et al., Chem. Mater. **21**, 2875 (2009)
25. A. Patterson, Phys. Rev. **56**, 978 (1939)
26. S. Kuriakose et al., Beilstein J. Nanotech. **4**, 763 (2013)
27. S. Musić, A. Šarić, Ceram. Int. **38**, 6047 (2012)
28. H. Zeng et al., Adv. Funct. Mater. **20**, 561 (2010)
29. E.S. Babu et al., Electron. Mater. Lett. DOI: 10.1007/s13391-014-4227-y
30. K. Park et al., J. Phys. Chem. C **115**, 20992 (2011)
31. Y. Konishi, I. Tanabe, T. Tatsuma, Dalton Trans. **42**, 15937 (2013)
32. F. Fabregat-Santiago et al., J. Phys. Chem. B **106**, 334 (2002)
33. F. Fabregat-Santiago et al., PCCP **8**, 1827 (2006)
34. C. Magne et al., J. Mater. Chem. A **1**, 2079 (2013)
35. J. Bisquert, PCCP **5**, 5360 (2003)